Eur. Phys. J. D (2018) 72: 127
https://doi.org/10.1140/epjd/e2018-90136-5

THE EUROPEAN PHYSICAL JOURNAL D

Regular Article

A closer insight into classical models for the He atom with two-active electrons

Nicolás Bachi[a] and Sebastian Otranto

Departamento de Física, Instituto de Física del Sur (IFISUR), Universidad Nacional del Sur (UNS), CONICET, Av. L. N. Alem 1253, B8000CPB Bahía Blanca, Argentina

Received 23 March 2018 / Received in final form 22 May 2018
Published online 5 July 2018

Abstract. In this work, two classical models which have been proposed to describe He atoms in collision processes by charged particle impact are revisited and analyzed. These are the Heisenberg-core and the energy-bounded classical trajectory Monte Carlo methods. These models avoid the classical autoionization by introducing in the Hamiltonian momentum-dependent terms. The physical implication of different choices of the involved parameters are analyzed as well as their influence at the total cross section level.

1 Introduction

The classical trajectory Monte Carlo method (CTMC), though initially developed by Abrines and Percival in 1966 [1], received much wider attention from the atomic collision physics community after the pioneering work on ion-atom collisions by Olson and Salop published nearly 40 years ago [2]. This work was soon after followed by others which rapidly highlighted the potential of this method to describe collision systems at impact energies at which quantum mechanical methods are difficult to implement due to large or incomplete basis-sets [3–5]. The methodology was presented to describe collisions of a charged projectile with a one-electron atom, i.e. a pure three-body process and provided, in conceptual terms, a computational counterpart of experimental procedures. In this context, the extension of the methodology to describe collision processes with He atoms was naturally the next and desirable step to provide grounds for more complex multielectronic targets. In contrast to the predictions of quantum mechanics, the classical He atom is unstable and autoionizes without the need of any external agent. To avoid the autoionization, different alternatives, like the Bohr atom [6], the neglect of the e–e interaction [7,8] and the backward–forward propagation scheme introduced by Geyer and Rost [9,10] have been considered. The Bohr atom model is stable as long as the projectile interacts for very short periods of time (i.e. very fast collisions) with the target. The models in which the e–e interaction is not explicitly considered can describe multielectronic processes in which the projectile interacts in sequential order with the electrons but fail to describe electronic emission mechanisms which rely on the e–e interaction. On the other hand, Geyer's approach initially propagates the target system backwards in time letting it autoionize. In a second stage the projectile-target interaction is turned on and the whole system is propagated forward, undoing the autoionization, so that in $t = 0$ the projectile encounters the refocused target in nearly its initial state. Up to our knowledge this model has not been pushed further and its viability for collisions involving highly charged projectiles and low impact energies must still be determined.

A different strategy was explored by Kirschbaum and Wilets [11] by adding momentum-dependent potential terms to the He atom Hamiltonian. These terms prevent the electrons to reach quantum-mechanically forbidden regions of phase space and provide stability to the target. This model has been used during the past three decades by different authors which have considered different sets of parameters for the momentum-dependent terms based on particular derivations [12–15]. Hereafter, we will generically refer to this model as the Heisenberg core CTMC model (HC-CTMC). In 1996, Cohen introduced the energy-bounded CTMC approach (EB-CTMC), in which energy constrain terms are introduced in the Hamiltonian to prevent electrons from falling to the He-nucleus [13]. The mentioned studies put emphasis in proton impact collisions with the exception of Cohen who also considered He^{2+} and Li^{3+} projectiles.

In recent years, there has been renewed interest in classical models for two-electron atoms. Models based on soft-core potentials have been considered with moderate success in the past decade as useful tools to get insight on double electron emission spectra in laser-atom studies [16,17]. Much more recently, the HC-CTMC model was used to provide a correlated picture of the double electron

[a] e-mail: nicolas.bachi@uns.edu.ar

emission in laser-argon studies[25pc] [18]. In this context, a critical evaluation of the main physical implications of these classical two-electron models seems necessary to correctly analyze future related studies.

In this work, we revisit the HC-CTMC and EB-CTMC models and study different sets of parameters to learn on their implications regarding the physical properties of the target. In Section 2, we present both models and focus on the ground state description (spatial extension and ionization energies). In Section 3, we focus on their implementation on the study of collisions processes following proton, C^{6+} and O^{8+} impact. In Section 4, we present our conclusions and outlook.

2 Target description

2.1 The HC-CTMC model

In this model the Hamiltonian is given by

$$H_{\rm HC} = H_0 + \sum_{i=1,2} V_{\rm H}(r_i, p_i). \tag{1}$$

In this expression H_0 represents the physical Hamiltonian

$$H_0 = \sum_{i=1,2} \left(\frac{p_i^2}{2} - \frac{Z}{r_i} \right) + \frac{1}{r_{12}}, \tag{2}$$

and the momentum-dependent potentials are parametrized as

$$V_{\rm H}(r_i, p_i) = \frac{\xi^2}{4\alpha r_i^2} \exp\left\{ \alpha \left[1 - \left(\frac{r_i p_i}{\xi} \right)^4 \right] \right\}. \tag{3}$$

Here, r_i and p_i are the position and canonical momentum of the ith electron, respectively.

The parameter α indicates the hardness of the constraint potentials and ξ is related to the size of the core. If $rp \leq \xi$, $V_{\rm H}$ becomes very repulsive and the electrons are not allowed to get close to the nucleus. In this sense, we note that different criteria have been used in the literature to provide explicit values for α and ξ. Cohen [13] showed that single capture and single ionization cross sections are much more sensitive to variations of ξ rather than α. In this sense, α can be considered a numerical parameter while ξ is a physical parameter. Following his analysis, we will then use a fixed value $\alpha = 2.0$ in what follows, a value that has been used in former studies [15,19]. By doing so, we will focus on the sensitivity of the physical properties of the target with respect to the ξ parameter. For this particular α-value, Cohen proposed $\xi = 0.9343$ with the aim of matching the first ionization potential of the target. Instead, Morita et al. [15] focused on obtaining a small core potential for the Bohr atom, and searched for the minimum ξ-value that would prevent autoionization. In their study, they proposed a marginal value of $\xi = 0.79$ which they consider close but safe from this limiting ξ-value. Much more recently, Zhou et al. [18] provided a different criterion to determine ξ in their laser-argon studies. For a given α, the ξ parameter is determined by asking the one-electron Hamiltonian

$$H_i^{\rm KW} = \frac{p_i^2}{2} - \frac{Z}{r_i} + V_{\rm H}(r_i, p_i), \tag{4}$$

to minimize at the second ionization potential of the two-electron atom. For He, and considering $\alpha = 2$, this criterion leads to $\xi = 0.894$ which corresponds to the exact second ionization potential of -2 a.u.

2.2 EB-CTMC

The second strategy under consideration is that proposed by Cohen [13]. In this model, the classical Hamiltonian for the two electron-atom is given by

$$H_{\rm EB} = H_0 + \sum_{i=1,2} V_{\rm EB}, \tag{5}$$

where H_0 is the same as in equation (2). Now, the constraint term is

$$V_{\rm EB} = \frac{Z}{r_i} \exp\left(\frac{E_0 - E_i^{\rm Coul}}{\Gamma} \right), \tag{6}$$

and it is applied to the one-electron Coulomb energy,

$$E_i^{\rm Coul} = \frac{p_i^2}{2} - \frac{Z}{r_i}. \tag{7}$$

The constants E_0 can be determinated by matching the minimum of the one-electron Hamiltonian,

$$H_i^{\rm EB} = E_i^{\rm Coul} + \frac{Z}{r_i} e^{(E_0 - E_i^{\rm Coul})/\Gamma}, \tag{8}$$

to the second ionization potential of the atomic target. The parameter Γ plays a similar role to that of α in the HC-CTMC model. In this sense, Γ can be considered a numerical parameter whereas E_0 is a physical parameter. Since the dependence on the Γ parameter is much weaker than on E_0 [13], we use $\Gamma = 0.3$ throughout our study. For this particular Γ, Cohen proposed $E_0 = -3.4$ a.u., a value that leads to $E_{\rm min} = -2.44$ a.u., that is -0.44 a.u. lower than the true binding energy of He^+. We have calculated that for this Γ, $E_0 = -2.91$ a.u. leads to $E_{\rm min} = -2.00$ a.u. This particular choice then provides a physical criterion comparable to that used by Zhou and collaborators within the HC-CTMC in their laser-atom studies.

2.3 Dynamics and target properties

Hamilton equations of motion for the system composed by the projectile and the two-electron target are numerically solved by means of a step adaptive Runge–Kutta–Gill method. The initial configuration in the phase space of the two-electron system is randomly generated so that its

energy equals the ground-state of He (−2.903 a.u.). The electronic coordinates $\mathbf{r_i}$ are generated with a probability distribution given by the radial distribution of the electrons that can be obtained from quantum mechanical Hartree–Fock wave functions. At this point, we determine the electrons momenta by inspecting $\mathbf{p_i}$ in the range (0, 5 a.u.) starting from very asymmetric geometries until a ground state energy within the range (−2.905 a.u., −2.902 a.u.) is obtained. Once determined their magnitudes the electrons momenta are randomly oriented. The system is then allowed to evolve for at least 100 a.u. of time before the projectile reaches the collision region. We have checked that similar cross sections are obtained when using Gaussian distributions instead of the quantum mechanical distributions in agreement with the statements of references [17,20].

In first place, we focus on the target dynamics of the two models explored by turning the projectile off. In Figure 1, we show the evolution of r_{12}^{-1} predicted by the HC-CTMC method for ξ in the range 0.7–0.894. The evolution of the He atom has been tracked for 10^4 a.u. of time. In all cases, energy conservation has been carefully tested throughout the simulation. In the figure, ξ-values lower than about 0.75 show clear trends of autoionization provided that r_{12}^{-1} tends to zero as the system evolves. On the other hand, for $\xi > 0.76$ the classical atom seems to be stable, and the range of r_{12}-values attainable shortens as this parameter increases. Based on the quantum mechanical radial distribution for the 1s orbital, one would expect a minimum r_{12}^{-1}-value of about 0.17 a.u. which is attained at the collinear configuration. However, since our classical description lacks tunnelling effects, the two-electron atom is expected to be contracted compared to its quantum mechanical counterpart. Hence, according to our results $\xi > 0.76$ should fulfill $r_{12}^{-1} > 0.17$ a.u. condition. Mean values for r_{12}^{-1} read 0.49 and 0.76 for $\xi = 0.76$ and $\xi = 0.78$ respectively. For $\xi = 0.894$, value at which the correct second ionization potential is recovered, r_{12}^{-1} oscillates with a mean value of 0.873 which is close to the value of 0.949 for $\langle 1/r_{12} \rangle$ predicted by a simple correlated variational wavefunction [21].

We perform a similar analysis for the EB-CTMC model in Figure 2. Two different values are chosen for E_0, namely −3.4 a.u. and −2.91 a.u. We observe that for the first value r_{12}^{-1} oscillates around the quantum mechanical $\langle 1/r_{12} \rangle$, while for the second value the interelectronic mean distance seems to be enlarged. Mean values for r_{12}^{-1} read 0.94 and 0.76 respectively exhibiting an inverse trend compared to HC-CTMC.

Now, we check the spatial distribution of electrons in both models. To provide an instantaneous picture of the $\mathbf{r_1}$, $\mathbf{r_2}$ and $\mathbf{r_{12}}$ coordinates, in Figures 3 and 4 we show ternary plots as initially proposed by Dalitz in 1953 [22]. In our case, we consider as ternary variables $\pi_{r_1} = r_1^2/(r_1^2 + r_2^2 + r_{12}^2)$, $\pi_{r_2} = r_2^2/(r_1^2 + r_2^2 + r_{12}^2)$ and $\pi_{r_{12}} = r_{12}^2/(r_1^2 + r_2^2 + r_{12}^2)$. These plots have been built by recording the r_1, r_2 and r_{12} values of each sorted event after a relaxation lapse of 100 a.u.

As expected, in all cases the spatial distribution is symmetric with respect to the median of the side $\pi_{r_{12}}$. Figures 3a and 3b correspond to the HC-CTMC with

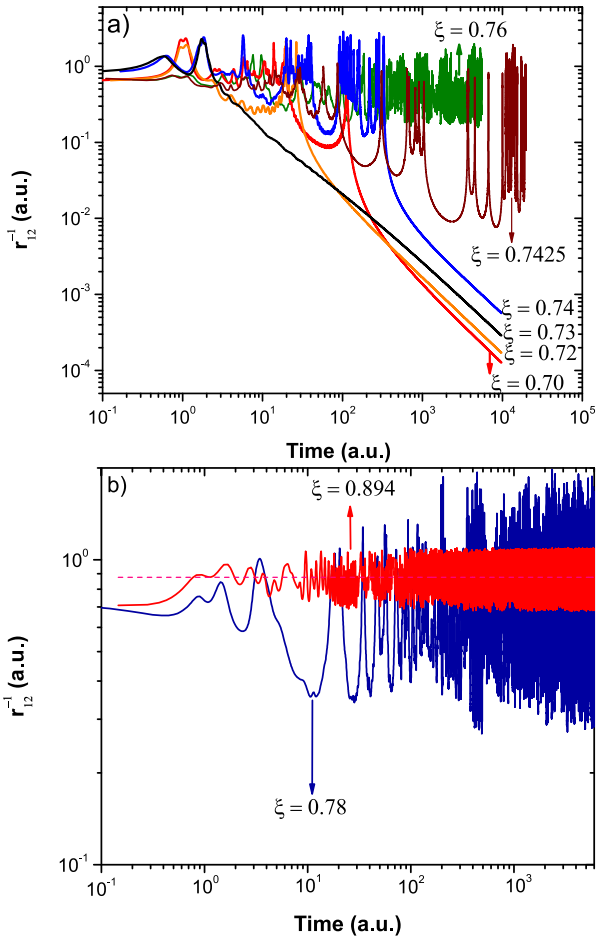

Fig. 1. Evolution of r_{12}^{-1} provided by the HC-CTMC model for different values of the ξ parameter.

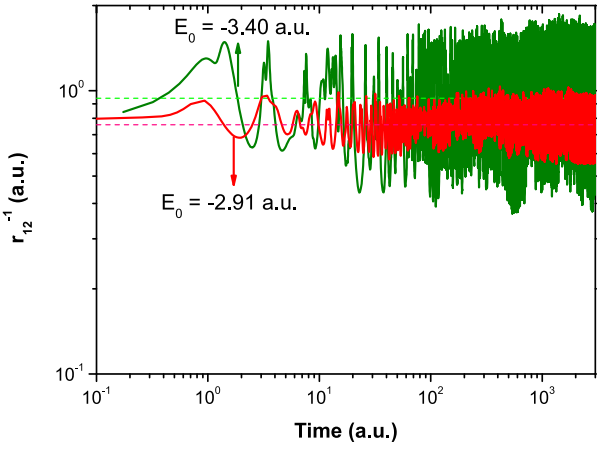

Fig. 2. Evolution of r_{12}^{-1} provided by the EB-CTMC model for different values of the E_0 parameter.

$\xi = 0.79$ and $\xi = 0.894$, respectively. In the first case, the points tend to accumulate close to the region where one of the parameter π_{r_i} $(i = 1, 2)$ is close to zero. This corresponds to the physical situation where one of the electrons is close to the nucleus while the other is distant. In this situation, the model predicts angles between $\mathbf{r_1}$ and

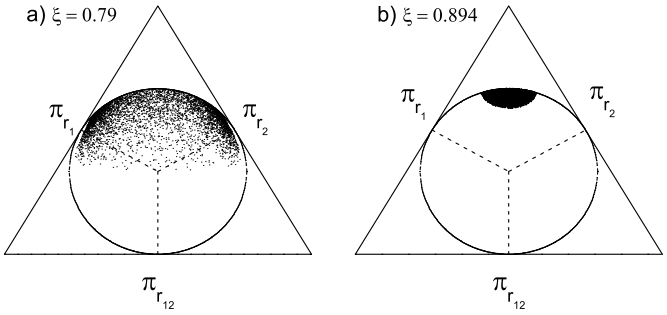

Fig. 3. Dalitz plots obtained from HC-CTMC with (a) $\xi = 0.79$; (b) $\xi = 0.894$.

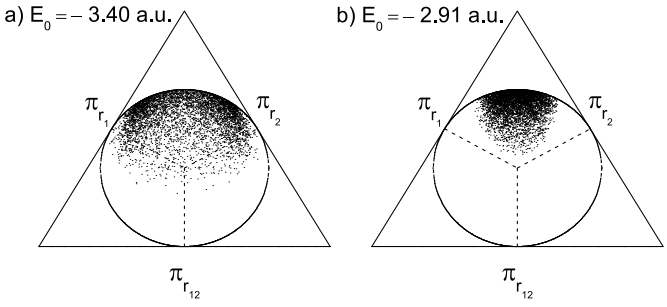

Fig. 4. Dalitz plots obtained from EB-CTMC with (a) $E_0 = -3.4$ a.u.; (b) $E_0 = -2.91$ a.u.

$\mathbf{r_2}$, $\theta_{12} > 40°$. In contrast, the second case shows that the electrons are at similar distances from the nucleus and $\theta_{12} \geq 115°$. This physical situation qualitatively resembles the spirit of the Bohr atom, since the electrons evolve at similar distances from the nucleus and use it to shield one another. The EB-CTMC method predicts a similar spatial distribution but more widespread than the HC-CTMC. When $E_0 = -3.4$ a.u. (Fig. 4a), there are points for which $\pi_{r_{12}}$ is lower than 1/3. In fact, from our simulation we found out that $\theta_{12} \geq 45°$. The second case (Fig. 4b) corresponds to $E_0 = -2.91$ a.u. and our simulation shows a major concentration in the upper third of the circumference ($\theta_{12} \geq 69°$).

We note that the physical parameters of both models (ξ and E_0) affect the electronic spatial distribution. This fact is not minor, provided that it will reflect in the range of impact parameters that will contribute for ionization processes.

Finally, and by turning the projectile on, we now gain insight into another important physical point that is the first and second ionization potentials predicted by these models when used within the simulation of atomic collision processes. To do so, we consider from our simulation the resulting single ionization events at a proton impact energy of 100 keV and record the binding energy of the remaining electron conforming the He^+ ion. The ionization potential is obtained by substracting that energy from the two-electron ground state binding energy of -2.9037 a.u. The results obtained for different ξ-values within the HC-CTMC are shown in Figure 5. It can be seen that for ξ-values close to the autoionization limit the first ionization potential of the target peaks at much lower values than 0.904 a.u. In consequence, the corresponding second ionization potentials are larger than the true value of -2.0 a.u. For $\xi = 0.894$, we observe that the first and second ionization potentials peak at the correct values providing a more accurate representation of the target. A similar analysis is shown in Figure 6 for the EB-CTMC model. Similar trends are observed in this case: $E_0 = -3.4$ a.u. leads to first (second) ionization potentials which are lower (larger) than the true values. On the other hand, $E_0 = -2.91$ a.u. leads to electron energy distributions which peak at the proper first and second ionization potentials of the He target.

3 Results

3.1 H^+ collisions with He

In first place we check the sensitivity of the single ionization (SI) and single capture (SC) cross sections to the ξ parameter in the 0.74–0.894 range. Results are shown in Figure 7. The experimental values of Shah and Gilbody [23] for SI and SC are indicated in terms of dashed lines. It can be seen that for $\xi = 0.76$ the single ionization (capture) cross section is overestimated (underestimated). This can be associated to the first ionization potentials value predicted for low ξ which clearly underestimate the true first ionization potential as stated above. As the ξ parameter increases in the range under consideration the theoretical predictions cross the experimental values and for $\xi = 0.894$, the more accurate model in terms of ionization potentials, the SI and SC cross sections are almost equal.

In Figure 8, we compare the total cross sections for SI, SC, transfer-ionization (TI), and double ionization (DI) predicted by the HC-CTMC for $\xi = 0.79$ and $\xi = 0.894$. The impact energy range explored was 10–3000 keV. In agreement with the results of Morita et al. [15], it can be seen that $\xi = 0.79$ predicts absolute values for SI and DI in good agreement with the data for impact energies >100 keV. Extension to lower impact energies, show that the SI cross section peaks at an impact energy of about 40 keV, while the data peaks at about 100 keV. This shift is already expected from long standing parameterizations [25] and can be related to the underestimation of the true first ionization potential for this particular ξ-value. In contrast, theoretical results obtained with $\xi = 0.894$ underestimate the SI channel in the entire energy range explored, but the shape of the cross section as a function of the impact energy is in much closer agreement to the data. It is worth noting that both models are expected to underestimate the single ionization experimental data in the high-energy limit provided that the classical cross section predict a $1/E$ behaviour in contrast to the $\log(E)/E$ expected from quantum mechanical treatments. Interestingly, the DI channel is similarly described by both models, probably related to the fact that the double ionization potential predicted by both models is the same. The SC channel is correctly described by both models for impact energies >30 keV, but we note that $\xi = 0.894$ provides the closest agreement for impact energies

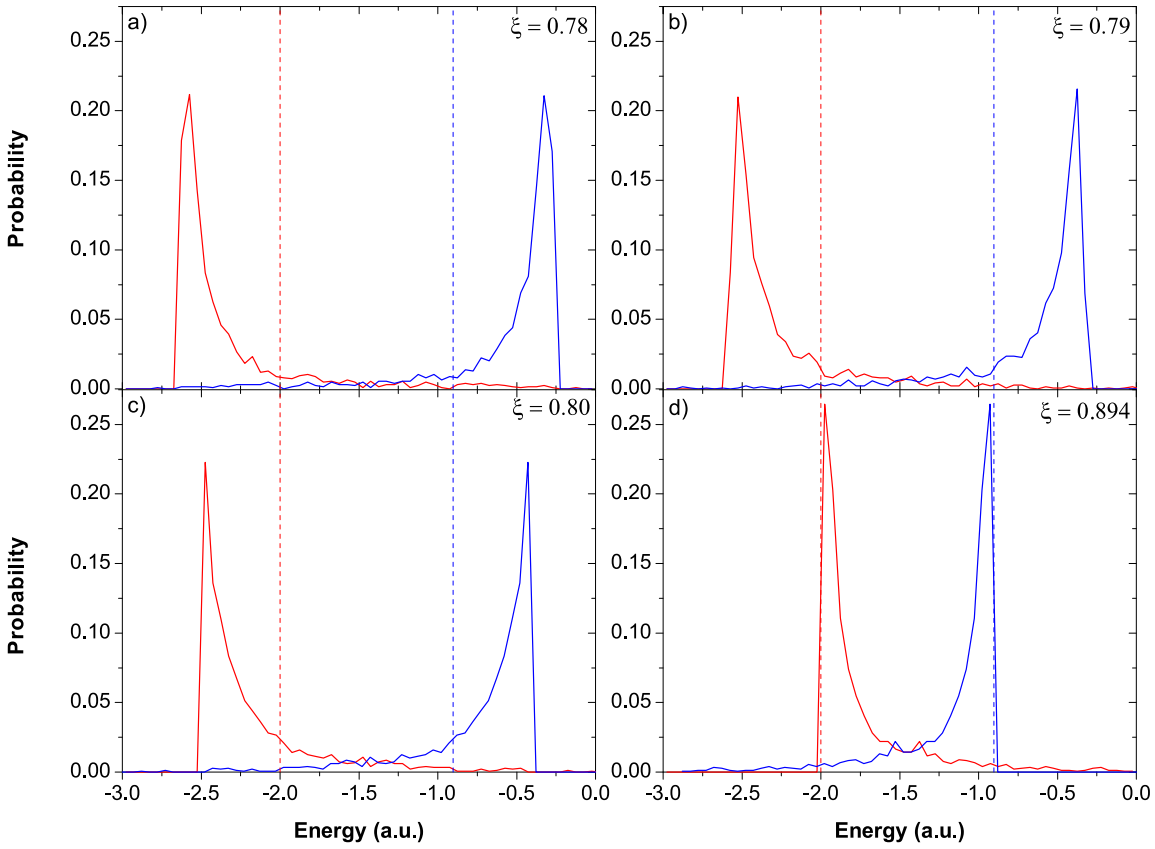

Fig. 5. HC-CTMC energy diagrams obtained from ionization events in 100 keV proton impact: (a) $\xi = 0.78$; (b) $\xi = 0.79$; (c) $\xi = 0.80$; (d) $\xi = 0.894$. Vertical dashed lines indicate the exact first and second ionization potentials for He.

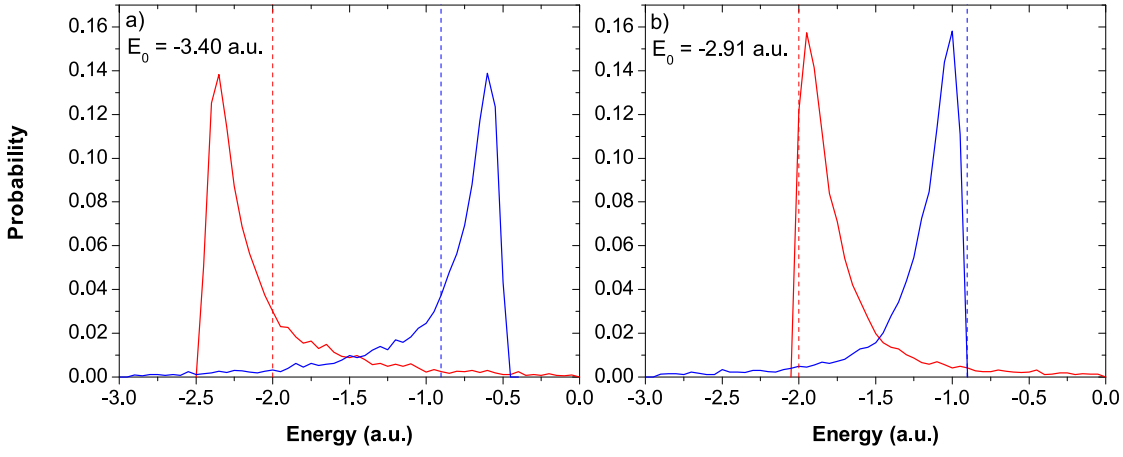

Fig. 6. EB-CTMC energy diagrams obtained from ionization events in 100 keV proton impact: (a) $E_0 = -3.4$ a.u.; (b) $E_0 = -2.91$ a.u. Vertical dashed lines indicate the exact first and second ionization potentials for He.

>200 keV. Finally, the TI cross sections for both models follow the trend of the experimental data for impact energies >40 keV, but clearly overestimate the data at lower impact energies. Preliminary results suggest that the overestimation of the TI cross section at impact energies <40 keV can be associated with capture events with binding energies exceeding 13.6 eV.

Figure 9 shows a similar analysis for the EB-CTMC model. In this case, results are shown for the two choices for the E_0 parameter that were discussed in Section 2.2, that is -3.4 a.u. and -2.91 a.u. For $E_0 = -3.4$ a.u., the SI cross section is in close agreement with the experimental data in nearly the whole range explored. The DI cross section peaks at about 100 keV, slightly overestimates that data for impact energies >100 keV but underestimates the cross section for impact energies <100 keV. SC is in very good agreement with the data for impact energies >20 keV. For $E_0 = -2.91$ a.u. the overall shapes

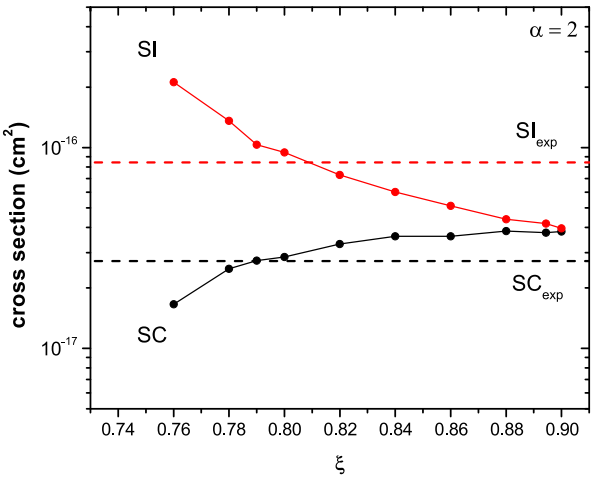

Fig. 7. 100 keV $H^+ + He$ cross section for single capture and ionization as a function of ξ. The dashed lines are experimental values for these cross sections [23].

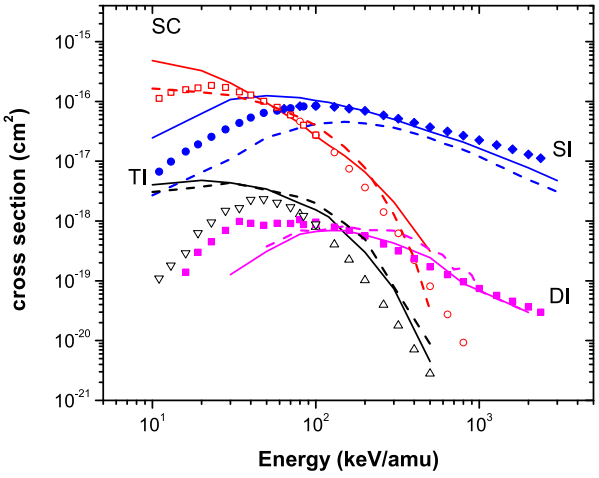

Fig. 8. HC-CTMC cross sections for single ionization (SI), single capture (SC), transfer-ionization (TI) and double ionization (DI) for $H^+ + He$ collisions as a function of impact energy, for $\xi = 0.79$ (solid line) and $\xi = 0.894$ (dashed line). Experimental data of Shah et al. [23,24] – open-squares and open-circles: SC; filled-circles and filled-diamonds: SI; open-down and open-up triangles: TI; and filled-squares: DI.

are similar to those obtained for $E_0 = -3.4$ a.u., but the SI magnitudes are lower in agreement with the trends observed for the HC-CTMC model. Finally, and for the same reason already stated, for both choices of the E_0 parameter the TI channel is overestimated in the whole energy range and the shape agreement with the data is similar to that obtained with the HC-CTMC model.

3.2 C^{6+} and O^{8+} collisions with He

Aside from the work of Cohen [13], which considers He^{2+} and Li^{3+} projectiles, up to our knowledge no other tests of the HC-CTMC and EB-CTMC models were performed for projectile involving larger charges. In this section we extend the analysis performed in the previous section and

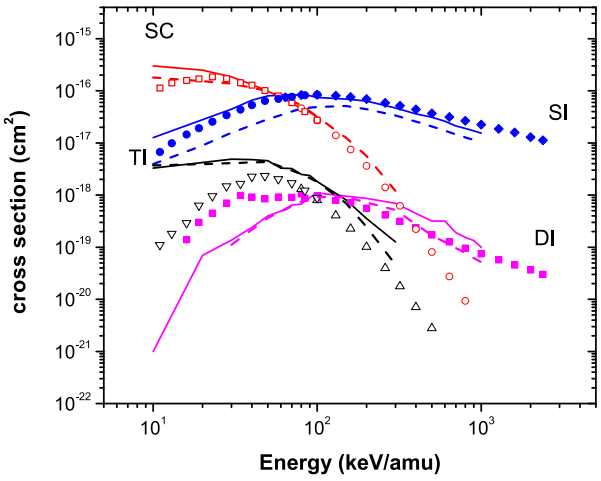

Fig. 9. EB-CTMC cross sections for single ionization (SI), single capture (SC), transfer-ionization (TI) and double ionizaion (DI) for $H^+ + He$ collisions as a function of impact energy, for $E_0 = -3.4$ a.u. (solid line) and $E_0 = -2.91$ a.u. (dashed-line). Experimental data of Shah et al. [23,24] – open-squares and open-circles: SC; filled-circles and filled-diamonds: SI; open-down and open-up-triangles: TI; and filled-squares: DI.

consider C^{6+} and O^{8+} projectiles. Focus of our analysis is made on the ratio σ_{SI}/σ_{SC} as a function of the impact energy. Present results are shown in Figures 10a and 10b and are contrasted to the experimental data of Wu et al. [26]. The HC-CTMC method with $\xi = 0.79$ and the EB-CTMC method with $E_0 = -3.4$ a.u. clearly overestimate the experimental data highlighting that the true first ionization potential is underestimated. Differences amount to nearly an order of magnitude throughout the entire energy range explored.

On the other hand, the HC-CTMC with $\xi = 0.894$ and the EB-CTMC with $E_0 = -2.91$ a.u. underestimate the experimental data but exhibit a much closer agreement. These trends indirectly reflects the fact that the underestimation of the first ionization potential leads to an increase in the range of impact parameters that feed the ionization channel, increasing in this sense the resulting total cross section.

4 Conclusions

In this work we have tested two classic models for the He atom which introduce momentum dependent potential terms in the Hamiltonian to avoid the classical unstability of the system. These models have been used in the literature for at least three decades by independent groups which have used different values for the numerical and physical parameters involved.

The focus of our study was twofold. On the one hand, we explored the physical implications of using different numerical values for these parameters. We have found that the first and second ionization potential strongly depend on the particular choice of parameters for both models. Such strong dependence reflects in the spatial distribution

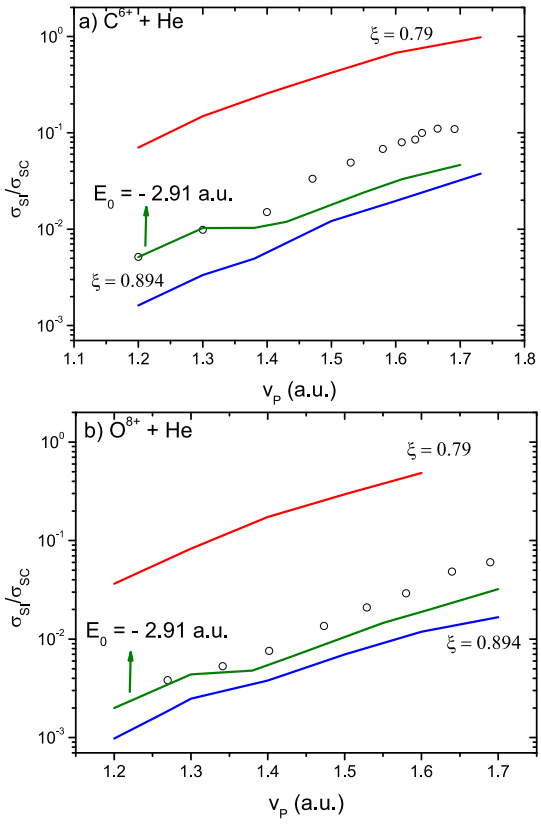

Fig. 10. HC-CTMC and EB-CTMC ratios of σ_{SI} to σ_{SC} as a function of impact energy for (a) $C^{6+} + He$; (b) $O^{8+} + He$. Experimental data of Wu et al. [26] (open-circles).

of the electrons as well. The HC-CTMC and EB-CTMC models with parameters that lead to the correct second ionization potential partially resemble Bohr-like dynamics (i.e. electrons orbiting the nucleus at quite similar radial distances and in a collinear configuration). In contrast, parameters which allow for deeper second ionization potentials, or lower first ionization potential values, seem to allow for more extended spatial distributions. In this case, orbits look much more asymmetric, with one electron near the nucleus and the other evolving at a larger distance.

Regarding our second objective, we have tested the sensitivity of the total cross sections for the different reaction channels to a particular choice of parameters. As a common trend, we have found that those models with an accurate description of the first and second ionization potentials, systematically underestimate the SI channel for proton impact. This could be due to the fact that weak collisions, where the projectile impact parameter is large, are poorly described in the classical treatment. The classical radial distribution of the target electrons have a characteristic cutoff and lack tunneling effects. In the three-body CTMC treatment, different authors worked upon developing phase-space functions which recover the quantum mechanical electron distribution for $H(1s)$ [27–29]. Similar analyses for $He(1s^2)$, in the context of the models hereby evaluated, remain to be performed. The SC channel, in contrast, seems to be less sensitive to the different models employed highlighting the fact that this channel is fed with events corresponding to inner impact parameters.

Present results for the SI/SC ratios for C^{6+} and O^{8+} collisions with He, suggest that the a correct description of the first and second ionization potentials could be particularly relevant as the projectile charge increases.

More work is needed in order to further determine the benefits and limitations of using these type of models to provide a classically correlated picture of two-electron ions. Moreover, the introduction of more general potentials between the electrons and the ion core would provide a route to infer the role of electron–electron correlation in more complex targets, such as multielectronic atoms or molecular targets, for which a correlated many-electron treatment of collision processes is actually lacking.

This work has been supported by PGI 24/F073, Secretaría General de Ciencia y Tecnología, Universidad Nacional del Sur (Argentina).

Author contribution statement

All the authors were involved in the preparation of the manuscript. All the authors have read and approved the final manuscript.

References

1. R. Abrines, I.C. Percival, Proc. Phys. Soc. Lond. **88**, 873 (1966)
2. R.E. Olson, A. Salop, Phys. Rev. A **16**, 531 (1977)
3. R.E. Olson, K.H. Berkner, W.G. Graham, R.V. Pyle, A.S. Schlachter, J.W. Stearns, Phys. Rev. Lett. **41**, 163 (1978)
4. R.E. Olson, Phys. Rev. A **24**, 1726 (1981)
5. R.A. Phaneuf, Phys. Rev. A **28**, 1310 (1983)
6. M.L. McKenzie, R.E. Olson, Phys. Rev. A **35**, 2863 (1987)
7. J.S. Cohen, Phys. Rev. A **36**, 2024 (1987)
8. A.E. Wetmore, R.E. Olson, Phys. Rev. A **38**, 5563 (1988)
9. T. Geyer, J.M. Rost, J. Phys. B: At. Mol. Opt. Phys. **36**, L107 (2003)
10. T. Geyer, J. Phys. B: At. Mol. Opt. Phys. **37**, 1215 (2004)
11. C.L. Kirschbaum, L. Wilets, Phys. Rev. A **21**, 834 (1980)
12. D. Zajfman, D. Maor, Phys. Rev. Lett. **56**, 320 (1986)
13. J.S. Cohen, Phys. Rev. A **54**, 573 (1996)
14. W.A. Beck, L. Wilets, Phys. Rev. A **55**, 2821 (1997)
15. S. Morita, N. Matsuda, N. Toshima, K. Hino, Phys. Rev. A **66**, 042719 (2002)
16. P.J. Ho, R. Panfili, S.L. Haan, J.H. Eberly, Phys. Rev. Lett. **94**, 093002 (2005)
17. S.L. Haan, L. Breen, A. Karim, J.H. Eberly, Phys. Rev. Lett. **97**, 103008 (2006)
18. Y. Zhou, C. Huang, Q. Liao, P. Lu, Phys. Rev. Lett. **109**, 053004 (2012)
19. J.S. Cohen, Phys. Rev. A **62**, 022512 (2000)
20. Y. Zhou, Q. Liao, P. Lu, Phys. Rev. A **80**, 023412 (2009)
21. S. Otranto, G. Gasaneo, C.R. Garibotti, Nucl. Instrum. Methods Phys. Res. B **217**, 12 (2004)

22. R.H. Dalitz, Philos. Mag. **44**, 1068 (1953)
23. M.B. Shah, H.B. Gilbody, J. Phys. B: At. Mol. Opt. Phys. **18**, 899 (1985)
24. M.B. Shah, P. McCallion, H.B. Gilbody, J. Phys. B: At. Mol. Opt. Phys. **22**, 3037 (1989)
25. I.D. Kaganovich, E. Startsev, R.C. Davidson, New J. Phys. **8**, 278 (2006)
26. W. Wu, C.L. Cocke, J.P. Giese, F. Melchert, M.L.A. Raphaelian, M. Stöckli, Phys. Rev. Lett. **75**, 1054 (1995)
27. D. Eichenauer, N. Grun, W. Scheid, J. Phys. B: At. Mol. Phys. **14**, 3929 (1981)
28. D.J.W. Hardie, R.E. Olson, J. Phys. B: At. Mol. Phys. **16**, 1983 (1983)
29. J.S. Cohen, J. Phys. B: At. Mol. Phys. **18**, 1759 (1985)